Effect of cooling rate on crystallization and magnetic properties of metallic $Co_{43}Fe_{20}Ta_{5.5}B_{31.5}$ glass

ZI-ZHOU YUAN*, XUE-DING CHENA, BING-XIA WANG
State Key Laboratory of Advanced Non-Ferrous Materials, Lanzhou University of Technology, Lanzhou, 730050, P.R. China
E-mail: yuanzz@lut.cn

ZI-JIANG CHEN
Jinchuan Nickel and Cobalt New Production Co., Jinchang, 73400, P.R. China

Published online: 12 April 2006

X-ray diffraction (XRD) and differential scanning calorimetry (DSC) were employed to investigate the effect of cooling rate on both non-isothermal and isothermal crystallization behavior of metallic $Co_{43}Fe_{20}Ta_{5.5}B_{31.5}$ glass. It is found that all DSC traces of the metallic $Co_{43}Fe_{20}Ta_{5.5}B_{31.5}$ glasses under different cooling rates exhibit one exothermic peak, which indicates that the crystallization of metallic $Co_{43}Fe_{20}Ta_{5.5}B_{31.5}$ glass follows a one-stage process. The XRD patterns of the metallic $Co_{43}Fe_{20}Ta_{5.5}B_{31.5}$ glasses under different cooling rates after non-isothermal DSC up to 1150 K show that all melt-spun ribbons of $Co_{43}Fe_{20}Ta_{5.5}B_{31.5}$ alloys produced under different cooling rates have the same precipitation phases after crystallization in the continuous heating DSC. In the case of non-isothermal crystallization process, the thermodynamic parameters are not affected by the cooling rate. During the isothermal annealing, the cooling rate also does not change the crystallization kinetics of metallic $Co_{43}Fe_{20}Ta_{5.5}B_{31.5}$ glass, but the nucleation rate in the whole crystallization process. The magnetic hysteresis loops measuring indicates that the values of saturation moment and coercivity exhibit correlation with the cooling rate.
© *2006 Springer Science + Business Media Inc.*

1. Introduction

The critical cooling rate is a very important factor that affects the formation of an amorphous phase. An important reason that a novel class of multi-component bulk metallic glasses (BMG) developed in recent years is formed easier than that of traditional metallic glasses can be partly attributed to the much lower critical cooling rate. However, since the first attempts to produce BMG by a variety of slow cooling techniques, some controversy arises concerning the structure of the resulting non-crystalline state [1]. The discrepancies refer to its stability, mechanical properties, corrosion resistance and magnetic properties connected to their use in applications as new engineering materials. Wang *et al*. [2] have studied the effect of cooling rate on crystallization of metallic $Zr_{70}Cu_{20}Ni_{10}$ glass, which indicates an existence of a close relationship between the cooling rate and thermodynamic parameters of crystallization. Damonte *et al*. [1] investigated the effect of preparation conditions on the short-range order in amorphous $Zr_{53}Hf_2Cu_{30}Al_{10}Ni_5$ and found that the short-range order in the as-prepared state was the same irrespective of the preparation method. It was also concluded that the crystallization process seemed to be not affected by the cooling rate. The effect of the rate of quenching from liquid on the structure and stability of amorphous $Co_{65}Fe_5Mo_2Si_{16}B_{12}$ alloy has been studied by Gupta *et al*. [3]. The results provide clear evidence of changes in topological short-range order with quenching rate. They also find that faster quenching rate results in an increased stability of the amorphous phase. $Nd_{60}Fe_{30}Al_{10}$ rapidly quenched foils and bulk samples were investigated by Bracchi *et al*. [4] and found to be structurally and magnetically inhomogeneous. Pinning processes between ferromagnetic and paramagnetic phases take place in the

*Author to whom all correspondence should be addressed.
0022-2461 © *2006 Springer Science + Business Media Inc.*
DOI: 10.1007/s10853-005-5600-x

slowly cooled sample as well as in the rapidly quenched one. But the strength of the pinning mechanisms depends strongly on the sample preparation, i.e. cooling rate.

The effect of cooling rate on crystallization and magnetic properties of Cobalt-based metallic glasses has not been extensively studied yet, especially for the new series of Co-Fe-Ta-B metallic glasses, which were recently reported by Inoue *et al*. [5–8]. The metallic $Co_{43}Fe_{20}Ta_{5.5}B_{31.5}$ (at.%) glass exhibits excellent glass forming ability, ultra-high strength above 5000 MPa and good soft magnetic properties. its maximum sample thickness (t_{max}) has reached as high as 2 mm that is the largest thickness for Co-based amorphous alloys reported up to now. The aim of this paper is to study the effect of cooling rate on the crystallization and magnetic properties of $Co_{43}Fe_{20}Ta_{5.5}B_{31.5}$.

2. Experimental

A master alloy with nominal composition of $Co_{43}Fe_{20}Ta_{5.5}B_{31.5}$ (at.%) were prepared by arc melting the mixtures of pure Co (99.8 mass%), Fe (99.95 mass%) and Ta (99.96 mass%) metals and pure crystalline B (99.9 mass%) in an water-cooled copper crucible under titanium-gettered argon atmosphere. The alloy ingots were re-melted several times to ensure homogeneity. Composition of the master alloy was verified with energy-dispersive X-ray spectroscopy. Melt-Spun ribbons with the same width of 4 mm and different thickness and cooling rate were fabricated by rapid solidification of the melt on a single copper roller at different wheel surface velocity under an air atmosphere.

Powder X-ray diffractometer (XRD) (X'Pertpro) using Cu K_α radiation was used to identify the amorphicity of the ribbons and the crystalline phases in the ribbons after continues heating DSC. Magnetic hysteresis loops were measured using a vibrating sample magnetometer (VSM) at room temperature. Both isothermal and non-isothermal DSC measurements were carried out using Perkin-Elmer Pyris Diamond TG/DTA calorimeter under flowing high purity N_2 (200 ml/min) to examine the thermal properties of the melt-spun ribbons. Temperature and energy calibrations of the instrument were performed using the well-known melting temperatures and melting enthalpies of high purity zinc and indium supplied with the instrument. The analyzed samples weighing about 34 mg, was cut into small pieces and, crimped in Al_2O_3 crucibles, where an empty Al_2O_3 pan was used as reference.

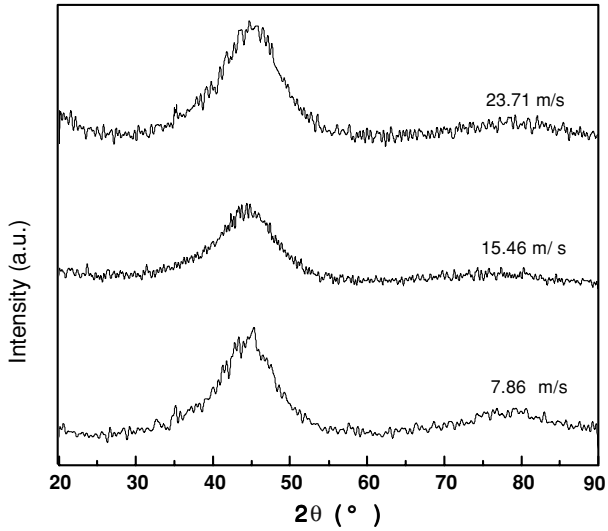

Figure 1 XRD patterns of melt-spun $Co_{43}Fe_{20}Ta_{5.5}B_{31.5}$ ribbons at different cooling rates

3. Results and discussion

The thickness of ribbons prepared at different wheel surface velocity is 132 μm for 7.86 m/s, 86 μm for 15.46 m/s and 65 μm for 23.71 m/s. Typical XRD patterns of metallic $Co_{43}Fe_{20}Ta_{5.5}B_{31.5}$ glasses produced under different cooling rates are shown in Fig. 1, in which only a broad diffraction peak in each pattern at the position of about $2\theta = 45^\circ$ can be observed, indicating fully amorphous. Fig. 2 shows the continuous heating DSC curves of metallic $Co_{43}Fe_{20}Ta_{5.5}B_{31.5}$ glasses taken at different heating rates, in which two separate reactions can be identified. The first reactions, which are endothermic, are due to the glass transition of the glassy phase, whereas the second sharp exothermic reaction is attributed to the single step crystallization of the glassy phase. We define the

TABLE I Thermodynamic parameters of metallic $Co_{43}Fe_{20}Ta_{5.5}B_{31.5}$ glass at different cooling rates

Parameters	Surface velocity (m/s)	10 K/min	25 K/min	45 K/min	65 K/min	90 K/min
T_g	7.86	910.4	921.3	922.4	924.6	929.6
	15.46	911.0	921.3	923.1	930.6	930.5
	23.71	910.1	919.5	925.2	927.4	932.6
T_x	7.86	961.2	974.3	982.8	990.1	996.2
	15.46	962	973.9	983.7	991.1	996.6
	23.71	962.9	974.9	983.4	990.3	997
T_P	7.86	968.2	982.1	993.2	1001.9	1008.3
	15.46	969.3	983.0	994.2	1001.8	1009.367
	23.71	969.6	982.8	992.6	1001.3	1010.1
ΔT_x	7.86	50.8	53	60.4	65.6	66.6
	15.46	51	52.6	60.6	60.5	66.1
	23.71	52.8	55.4	58.2	62.9	64.4

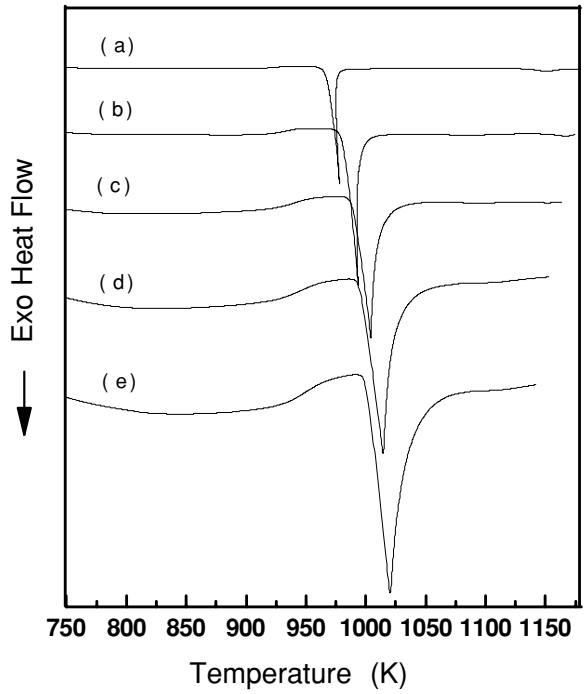

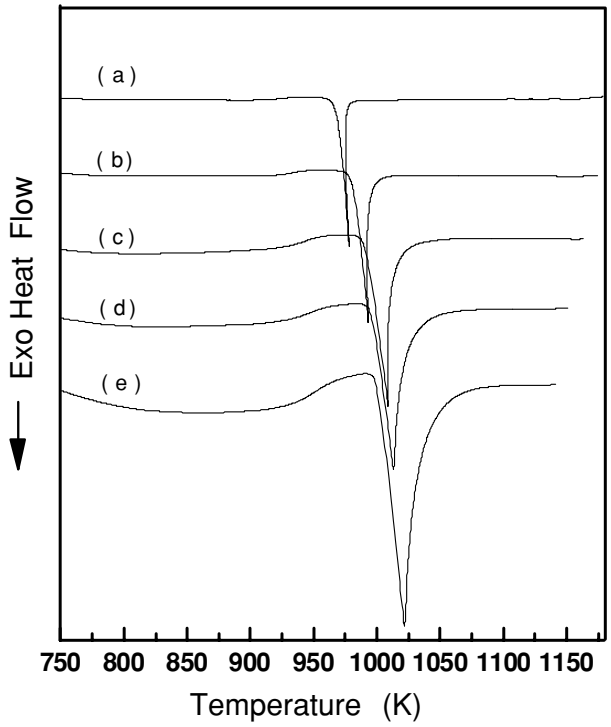

Figure 2 DTA traces of metallic $Co_{43}Fe_{20}Ta_{5.5}B_{31.5}$ glass taken at (a) 10 K/min, (b) 25 K/min, (c) 45 K/min, (d) 65 K/min, and (e) 85 K/min, respectively. (2–1), (2–2) and (2–3) represent the $Co_{43}Fe_{20}Ta_{5.5}B_{31.5}$ melt-spun ribbon obtained at a surface velocity of 7.86, 15.46 and 23.71 m/ s, respectively.

onset temperature of first and second reactions as glass transition, T_g and crystallization, T_x temperatures, respectively. In addition, the supercooled liquid region prior to crystallization, will be denoted as ΔT_x ($\Delta T_x = T_x - T_g$). The values of T_g, T_x, T_p (peak temperature) and ΔT_x at different heating rates for metallic $Co_{43}Fe_{20}Ta_{5.5}B_{31.5}$ glasses under different cooling rates are summarized in

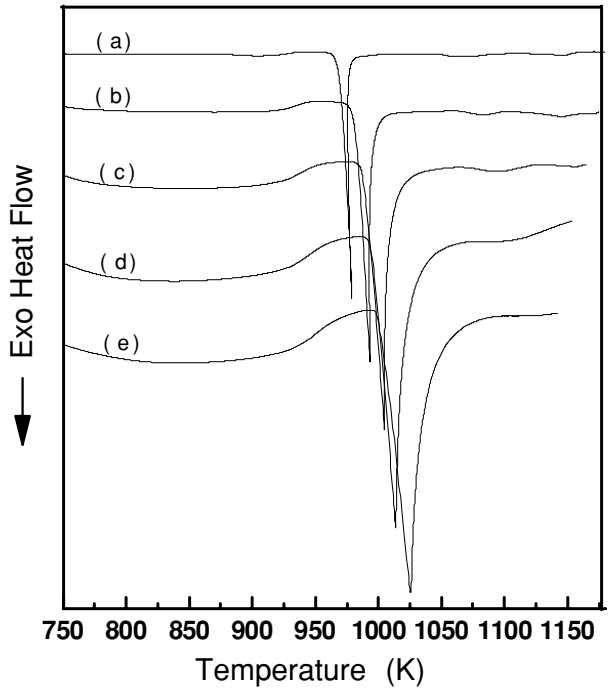

Figure 2 Continued.

Table I. It can be noted that T_g, T_x and T_p are shifted to higher temperatures and the value of ΔT_x increases along with heating rate for a fixed cooling rate, which implies that both the crystallization and glass transition of the metallic $Co_{43}Fe_{20}Ta_{5.5}B_{31.5}$ glasses display a dependence on the heating rate during continuous heating. Therefore, the thermal stability of the metallic $Co_{43}Fe_{20}Ta_{5.5}B_{31.5}$ glasses cannot be characterized by a definite critical temperature independent of the heating rate. It can also be seen that within the experimental error, the cooling rate does not have a significant effect on the values of T_g, T_x, T_p and ΔT_x at different heating rates, suggesting that the glassy phases formed under different cooling rates are identical in structure and homogeneous in composition. Fig. 3 shows XRD patterns of the melt-spun $Co_{43}Fe_{20}Ta_{5.5}B_{31.5}$ ribbons obtained under different cooling rates after non-isothermal DSC up to 1150 K. It is seen that all melt-spun ribbons of $Co_{43}Fe_{20}Ta_{5.5}B_{31.5}$ alloys produced under different cooling rates have the same precipitation phases after crystallization in the continuous heating DSC. According to Ref. [5], the structure after crystallization is consisted of the (Co,Fe)B and $(Co, Fe)_3B_2$ phases.

The activation energy for the crystallization E_c of metallic $Co_{43}Fe_{20}Ta_{5.5}B_{31.5}$ glasses in the condition of continuous heating can be obtained on the basis of the Kissinger equation [9]:

$$\ln\left(T_p^2/\beta\right) = E_c/RT_p + \text{constant} \qquad (1)$$

where T_p stands for the exothermic peak temperature, β the heating rate, E_c the activation energy for crystallization, and R the gas constant. By using the values of T_p and β listed in Table I, a plot of$\ln(T_p^2/\beta)$ vs. $1/T_p$

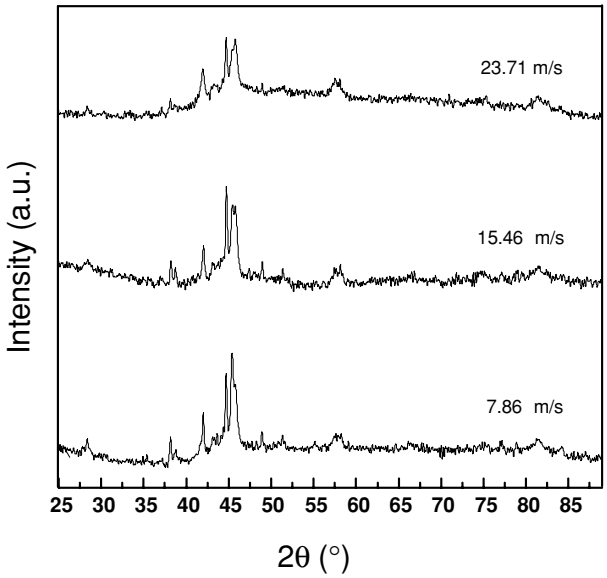

Figure 3 XRD pattserns of melt-spun $Co_{43}Fe_{20}Ta_{5.5}B_{31.5}$ ribbons obtained at different cooling rates after non-isothermal DSC up to 1150 K.

yields approximately straight lines as shown in Fig. 4. According to the slope of these straight lines, the activation energy for crystallization are obtained. It is estimated that the activation energy for crystallization of metallic $Co_{43}Fe_{20}Ta_{5.5}B_{31.5}$ glasses produced at 7.86, 15.46 and 23.71 m/s are 428.76, 434.85, and 431.75 kJ/mol, respectively. The small change of E_c for the different cooling rates is attributed to the experimental error. Therefore, it can be conclude that the cooling rate does not have a significant effect on the activation energy for crystallization of metallic $Co_{43}Fe_{20}Ta_{5.5}B_{31.5}$ glass.

The isothermal crystallization kinetics of metallic $Co_{43}Fe_{20}Ta_{5.5}B_{31.5}$ glass in the supercooled liquid region was further investigated with DSC at the temperature of

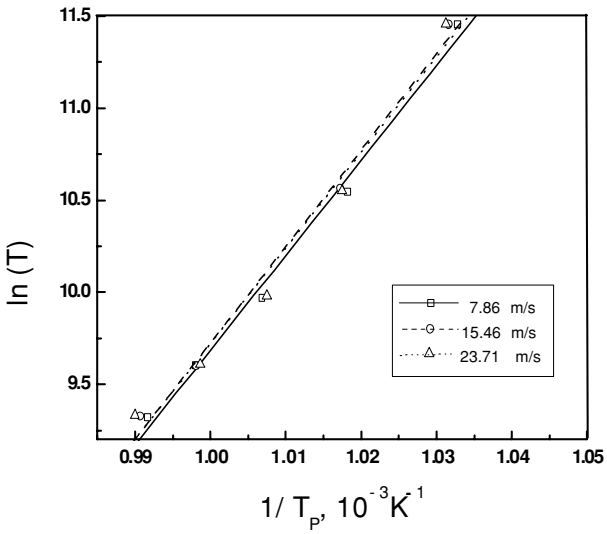

Figure 4 The correlation between $1/T_P$ and ln (T_P^2/β) of metallic $Co_{43}Fe_{20}Ta_{5.5}B_{31.5}$ glasses formed under different cooling rates.

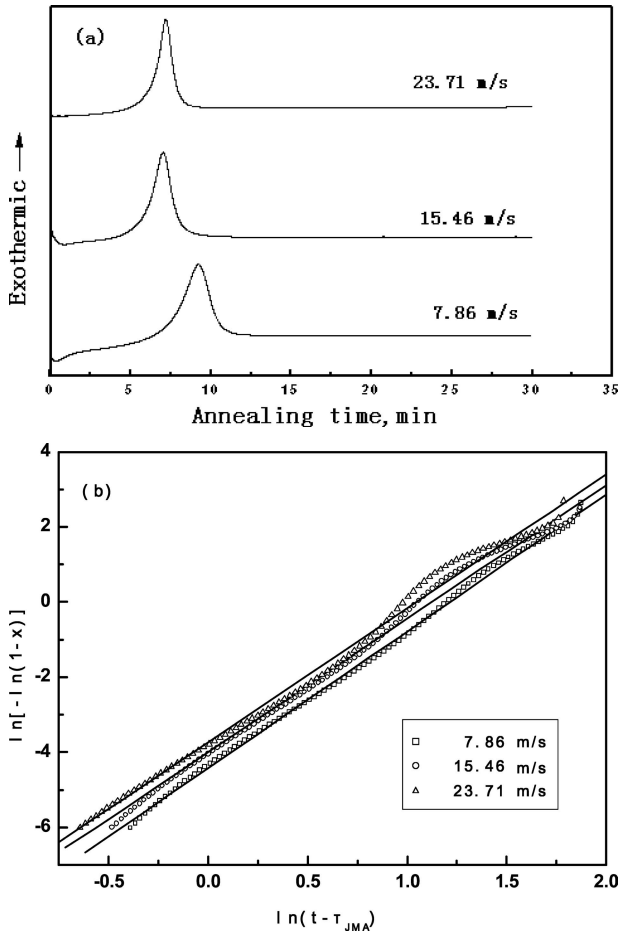

Figure 5 (a) Isothermal DSC curves and (b) JMA Plots at 950 K for metallic $Co_{43}Fe_{20}Ta_{5.5}B_{31.5}$ glasses produced under different cooling rates.

950 K, and the DSC plots corresponding for different cooling rates are shown in Fig. 5a. Similar to continuous heating, All of the isothermal DSC traces show a single crystallization process after a certain incubation period.

According to the theoretical Johnson-Mehl-Avrami (JMA) nucleation and growth kinetic [10, 11], the crystallization transformed fraction x is given by:

$$x(t) = 1 - \exp[-(kt)^n] \qquad (2)$$

where $x(t)$ is the crystallized volume fraction (%), which is obtained by measuring the area under the peak of isothermal DSC trace at different times and dividing them by the total area. n is the Avrami exponent, reflecting the characteristics of nucleation and growth during crystallization, and k is the Arrhennius temperature-dependent reaction rate constant. Equation 2 has generally been accepted also for the crystallization of metallic glasses. Generally, addition corrections to the ideal JMA law have to be assumed to fit the experimental data well.

In the isothermal case, to linearize the measured time dependence of x obeying JMA kinetics according to ln $[-\ln\,(1-x(t)) = n\,\ln\,k + n\,\ln\,(t-\tau_{\mathrm{JMA}})$, some time lag τ_{JMA} has to be subtracted from the real experimental

time t. Thomson *et al*. [12] have shown that such modification of JMA nucleation and growth law is consistent with the introduction of the transient nucleation effect in the early stages of crystallization. From the isothermal measurements (see Fig. 5(a)), the following results were obtained using the best correlation coefficient, r, to determine the optimal JMA exponent, n for $0.25 < x < 100\%$ (see Fig. 5(b)):

$$n_1 = 3.639, \quad t_1 = 362.8\,\text{s},$$
$$r = 0.99895 \text{ for the glass produced at } 7.86\,\text{m/s}$$

$$n_2 = 3.558, \quad t_2 = 256.3\,\text{s},$$
$$r = 0.9951 \text{ for the glass prepared at } 15.46\,\text{m/s}$$

$$n_3 = 3.569, \quad t_3 = 275.8\,\text{s}, \textit{nonumber}$$
$$r = 0.9936 \text{ for the glass formed at } 23.7\,\text{m/s}$$

The almost identical values of n for crystallization of metallic $Co_{43}Fe_{20}Ta_{5.5}B_{31.5}$ glasses produced at different cooling rates indicates that the isothermal crystallization of the metallic $Co_{43}Fe_{20}Ta_{5.5}B_{31.5}$ glass is independent of cooling rate, and dominated by decreasing nucleation rate under interface-controlled three-dimensional growth of nuclei [13].

It is widely accepted that the nucleation and growth do not remain constant during the whole crystallization process of an amorphous alloy. In order to investigate the influence of cooling rate on the details of the isothermal crystallization process, the local Avrami exponent $n(x)$ was calculated using the following equation [14]:

$$n(x) = d\ \ln[-\ln(1-x)]/d\ \ln(t - T_{\text{JMA}}) \qquad (3)$$

The value of $n(x)$ gives information on the nucleation and growth behavior when the crystallized volume fraction is x. Fig. 6 shows the relationship between the local Avrami exponent, $n(x)$, and crystallized volume fraction, x, at 950 K. It is seen from Fig. 6 that all curves exhibit a similar tendency with crystallized volume fraction. In the case of 23.71 m/s, $n(x)$ exceeds 4 when x falls into the range of 21∼87%, indicating that nucleation rate turns from the decreasing to the increasing, whereas the range of x shrinks slightly to 21∼83% in the case of 15.46 m/s, However, it farther shrinks to $32 < x < 83.5\%$ in the case of 7.86 m/s. The maximum values of n for 23.71, 15.46 and 7.86 m/s are 5.979, 5.18 and 4.17, respectively. This behavior illustrates that the crystallization kinetics of metallic $Co_{43}Fe_{20}Ta_{5.5}B_{31.5}$ glass is independent of the cooling rate but the crystallization process, i.e., the nucleation rate in the whole crystallization process is strongly correlated to the cooling rate in the condition of isothermal annealing. It is understandable that, as that the size of

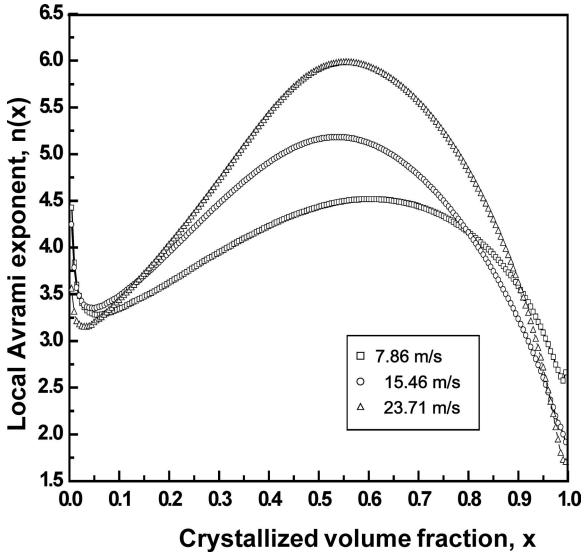

Figure 6 Variation of the Avrami exponents with crystallized fraction for metallic $Co_{43}Fe_{20}Ta_{5.5}B_{31.5}$ glasses obtained at different cooling rates.

short-range order increases while cooling rate decreases, the probability of the short-range order acting as pre-existing nuclei is larger, and the new nuclei forming rate is lower in the case of low cooling rate.

The difference of nucleation and growth behavior during crystallization is also reflected in the variation of the activation energy in different crystallization stages. On the basis of the dynamic DSC measurements at various heating rates the isoconversional method of Kissing, Akahira and Sunose was used [15]. This is a model free method which involves measuring the temperatures, T_f corresponding to fixed values of the crystallization volume fraction x, from experiments at different heating rates, β, and plotting $\ln(\beta/T_f^2)$ against $1/T_f$

$$\ln(\beta/T_f^2) = -E_c(x)/RT_f + \text{constant} \qquad (4)$$

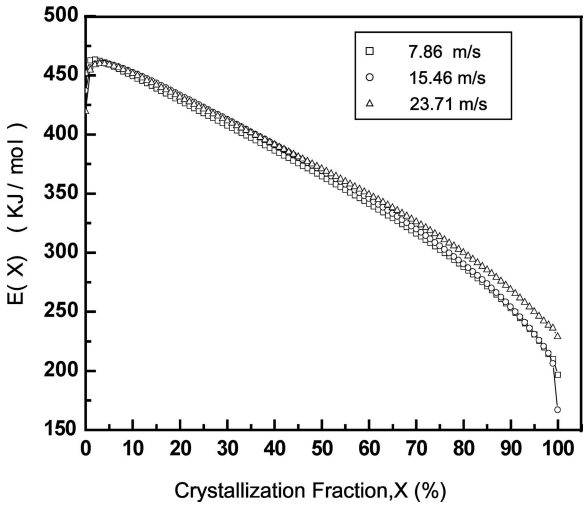

Figure 7 Variation of activation energy during crystallization process for metallic $Co_{43}Fe_{20}Ta_{5.5}B_{31.5}$ glasses at different cooling rates.

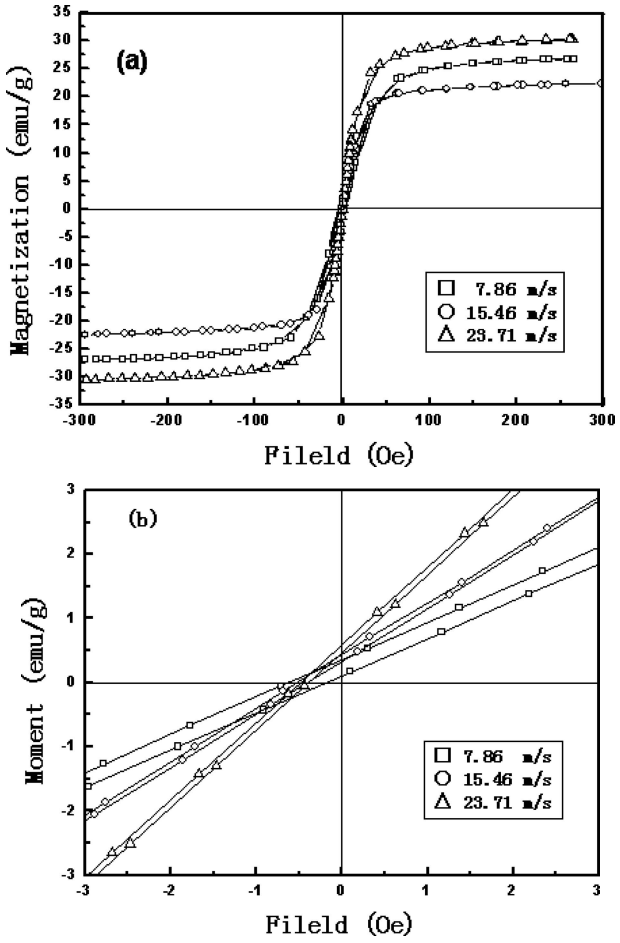

Figure 8 >Room-temperature magnetic hysteresis loops for metallic $Co_{43}Fe_{20}Ta_{5.5}B_{31.5}$ glasses produced under different cooling rates: (a) full ranged and (b) in another scale, which clarifies the coercivity.

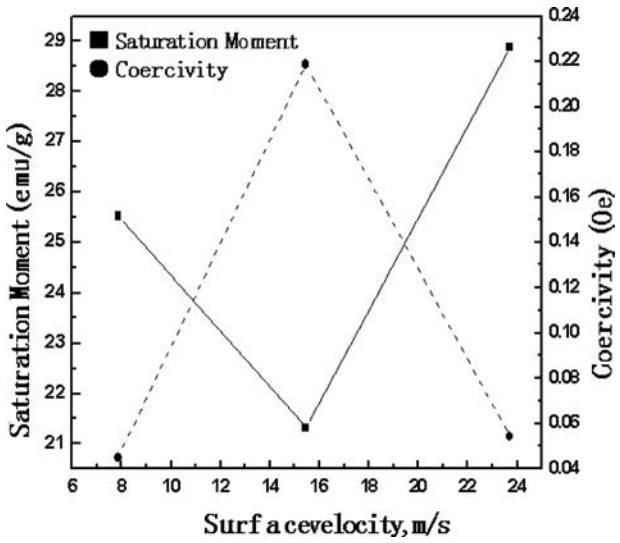

Figure 9 Variation of the saturation moment and coercivity with cooling rates for metallic $Co_{43}Fe_{20}Ta_{5.5}B_{31.5}$ glass.

And the slopes of such plots give $-E_c$ $(x)/R$. Fig. 7 shows the plot of E_c (x) vs. x for the metallic $Co_{43}Fe_{20}Ta_{5.5}B_{31.5}$ glasses under different cooling rates, from which the variation of E_c (x) with x is evident, indicating a complex crystallization mechanism that invalidates the separation of variables involved in the KAS analysis [16]. The curves corresponding to different cooling rates are almost overlapped, suggesting that the crystallization of metallic $Co_{43}Fe_{20}Ta_{5.5}B_{31.5}$ glasses is independent of the cooling rate under the non-isothermal condition.

Fig. 8 plots the respective magnetic hysteretic loops for the metallic $Co_{43}Fe_{20}Ta_{5.5}B_{31.5}$ glasses under different cooling rates. These curves are plotted in the two applied magnetic field ranges: (a) $\pm$300 Oe and (b) $\pm$3 Oe. It can be seen that metallic $Co_{43}Fe_{20}Ta_{5.5}B_{31.5}$ glasses under different cooling rates have excellent soft magnetic properties. As shown in Fig. 9, the values of saturation moment and coercivity apparently correlated with the cooling rate. The saturation moment decreases firstly, and reaches a minimum at the surface velocity is 15.46 m/s, and then increases along with the surface velocity, whereas, the coerceivity increases firstly, and reaches a maximum at the same surface velocity, and then decrease along with the surface velocity. This was attributed to the larger stress induced at such surface velocity, which influences magnetic properties [9].

4. Conclusions

The effect of cooling rate on the crystallization and magnetic properties of metallic $Co_{43}Fe_{20}Ta_{5.5}B_{31.5}$ glass has been investigated. It is found that the thermodynamic parameters and precipitation phases are not affected by the cooling rate in the case of non-isothermal crystallization process, whereas in the case of isothermal annealing, though the cooling rate has little effect on the crystallization kinetics of the glass, it affects nucleation rate in the whole crystallization process. The measurements of magnetic hysteresis loops indicate that the saturation moment and coercivity apparently correlates with the cooling rate.

Acknowledgments

This work was supported by the Hi-tech Research and Development Program of China (863), grant no. 2003 AA32 X150

References

1. L.C. DAMONTE, L. A. MENDOZA-ZÉLIS, S. DELEDDA and J. ECKERT, *Mater. Sci. Eng. A* **343** (2003) 194.
2. H. R. WANG, Y. L. GAO, X. D. HUI, Y. CHEN, G. H. MIN and Y. F. YE, *J. Alloys Comp.* **350** (2003) 178.
3. A. GUPTA and M. JAYARAJ, *J. Non-cryst. Solids.* **149** (1992) 275.
4. A. BRACCHI, S. SCHNEIDER, P. THIYAGARAJAN and K. SAMWER, *J. Magn. Magn. Mater.* **272–276** (2004) 1423.
5. A. INOUE, B.L. SHEN, H. KOSHIBA, H. KATO and A.R. YAVARI, *Acta Mater.* **52** (2004) 1631.

6. *Idem*., *Nature Mater*. **2** (2003) 661.
7. B. L. SHEN, H. KOSHIBA, A. INOUE, H. KIMURA and T. MIZUSHIMA, *Mater. Trans. JIM*. **42** (2001) 2136.
8. H. KOSHIBA and A. INOUE, *ibid*. **42** (2001) 2572.
9. H. E. KISSINGER, *Anal. Chem*. **29** (1957) 1702.
10. M.A. JOHNSON and R. F. MEHL, *Am. Inst. Metall. Pet. Eng*. **135** (1939) 416.
11. M. AVRAMI, *J. Phys. Chem*. **7** (1939) 1103.
12. C.V. THOMPSON, A. L. GREER and F. SPAEPEN, *Acta Metall*. **31** (1983) 1883.
13. M J. STARINK, *J. Mater. Sci*. **36** (2001) 4433.
14. N. X. SUN, K. ZHANG, X. H. ZHANG, X. D. LIU and K. LU, *Nanostruct. Mater*. **7** (1996) 637.
15. M J. STARINK, *Thermochim. Acta*. **404** (2003) 163.
16. K. CHRISSAFIS, *ibid*. **411** (2004) 7.

Received 12 February
and accepted 18 July 2005